Numerical simulation of 2D Silicon MESFET and MOSFET described by the MEP based energy-transport model with a mixed finite elements scheme

A.M. Anile, Americo Marrocco, V. Romano, J.M. Sellier

INRIA

INSTITUT NATIONAL DE RECHERCHE EN INFORMATIQUE ET EN AUTOMATIQUE

Numerical simulation of 2D Silicon MESFET and MOSFET described by the MEP based energy-transport model with a mixed finite elements scheme

A.M. Anile and A. Marrocco and V. Romano and J.M.Sellier

N° 5095

Janvier 2004

THÈME 4

ISSN 0249-6399 ISRN INRIA/RR--5095--FR+ENG

INRIA
ROCQUENCOURT

Numerical simulation of 2D Silicon MESFET and MOSFET described by the MEP based energy-transport model with a mixed finite elements scheme

A.M. Anile* and A. Marrocco† and V. Romano‡ and J.M.Sellier*

Thème 4 — Simulation et optimisation
de systèmes complexes
Projet Bang

Rapport de recherche n° 5095 — Janvier 2004 — 28 pages

Abstract: The Mixed Finite Element approximation scheme presented in [1] is used to simulate a consistent hydrodynamical model for electron transport in semiconductors, free of any fitting parameters, formulated on the basis of the maximum entropy principle (MEP) in [2, 3, 4].

2D-MESFET and 2D-MOSFET Silicon devices are simulated in the parabolic band approximation. Comparison with the results obtained by the Stratton model are presented for completeness.

Key-words: numerical simulation, mixed finite element, MESFET and MOSFET semiconductor devices, maximum entropy principle, parabolic band approximation, automatic differentiation

* Dipartimento di Matematica e Informatica, Università di Catania, Viale A.Doria 6, I-95125 Catania, Italy
† Inria, Domaine de Voluceau, Rocquencourt BP 105 78153 Le Chesnay, France
‡ Facoltà di Ingegneria sede di Enna, Dipartimento di Matematica e Informatica, Università di Catania, Viale A.Doria 6, I-95125 Catania, Italy

Unité de recherche INRIA Rocquencourt
Domaine de Voluceau, Rocquencourt, BP 105, 78153 Le Chesnay Cedex (France)
Téléphone : +33 1 39 63 55 11 — Télécopie : +33 1 39 63 53 30

Simulation bidimensionnelle à l'aide des éléments finis mixtes de dispositifs semi-conducteurs au silicium (MESFET et MOSFET) décrits par un modèle energy-transport basé sur le principe d'entropie maximum

Résumé : Le schéma d'approximation utilisant les éléments finis mixtes et présenté en [1] est utilisé pour simuler un modèle hydrodynamique consistant de transport d'électrons dans les matériaux semi-conducteurs, modèle exempt de tout lissage de paramètres et formulé sur la base du principe d'entropie maximum (abrégé en MEP pour *Maximum Entropy Principle*), voir [2, 3, 4].

Des dispositifs semi-conducteurs de type MESFET et MOSFET ont été simulés en considérant l'approximation parabolique classique des bandes d'énergie. Les résultats obtenus sont comparés à ceux obtenus avec le modèle de Stratton.

Mots-clés : simulation numérique, éléments finis mixtes, dispositifs semi-conducteurs MESFET et MOSFET, principe d'entropie maximum, approximation parabolique des bandes d'énergie, différentiation automatique

1 Introduction

In today semiconductor technology, the miniaturization of the devices is more and more progressing. As a consequence, the simulation of submicron semiconductor devices requires advanced transport models. Because of the presence of very high and rapidly varying electric field, phenomena occur which cannot be described by means of the well-known drift-diffusion models, which does not incorporate energy as a dynamical variable. That is why some generalization has been sought in order to obtain more physically accurate models, like energy-transport and hydrodynamical models. The energy transport models which are implemented in commercial simulators are based on phenomenological constitutive equations for the particle flux and energy flux depending on a set of parameters which are fitted to homogeneous bulk material Monte Carlo simulations. However, a more satisfactory physical description should be based on relating the parameters appearing in the constitutive laws to the fundamental scattering properties of electrons with phonons and impurities [6]. In [2, 3, 4] a model free of any fitting parameters has been developed for the electron transport in silicon, where the parameters appearing in the constitutive laws are directly related to the collision operators of the semiclassical Boltzmann transport equations for electrons in semiconductors. It is based on the maximum entropy principle, takes into account all the relevant scattering mechanisms in Silicon, e.g. scattering of electrons with acoustic and non-polar phonons and with impurities, and holds also for non-parabolic bands. The model is represented, apart from the Poisson equation for the electric potential, by a hyperbolic quasilinear system of balance law. In [4], it has been shown that it is possible to recover an energy-transport limiting model which is equivalent in the stationary case to the original one, al least for smooth solutions, and which is now parabolic.

The model has been tested in one dimensional problems, like n^+-n-n^+ diodes, in [4] while in [5] a 2D-MESFET has been simulated. In all these simulations a finite difference numerical method has been used.

Here we use the energy-transport formulation of the model for simulating the steady state of a 2D-MESFET and a 2D-MOSFET silicon device. In the present paper only the parabolic band case will be considered. In a forthcoming article the case when the energy bands are described by the Kane dispersion relation will be presented.

At variance with [5] the numerical scheme is based on mixed finite elements which guarantee accurate current conservation and also allow to deal with very complex geometry domains. For the theoretical details of the scheme the interested reader is referred to [1, 7, 8]. The method is very stable and robust and has previously been used for the simulation of other energy-transport models, like those derived by the spherical harmonic expansion [9, 10], that proposed by Chen et al [11] and by Lyumkis et al [12] and the Stratton one [13].

The plan of this paper is as follow. In the second section we give a brief presentation of the model. In section 3, the model is put in a form suitable for the numerical scheme which is presented in section 4. The last two sections are devoted to the numerical results for the MESFET and MOSFET. For the sake of completeness some comparisons with the Stratton model will be also shown.

2 The MEP Energy-Transport Model

In this section we give only a brief sketch of the Energy-Transport model which we will use, and, we briefly show how to recover this from the MEP hydrodynamical model. We limit our discussion to the parabolic band case. For more details and for the nonparabolic band case the interested reader is referred to [2, 3, 4].

We assume that the conduction band is described around each minimum (valley) by the parabolic band approximation

$$\mathcal{E}(\mathbf{k}) = \frac{\hbar^2 k^2}{2m^*}, \qquad \mathbf{k} \in \mathbf{R^3} \tag{1}$$

where $\mathcal{E}$ is the electron energy, m^* is the effective electron mass (which is 0.32 m_e in Silicon, with m_e the electron mass in the vacuum), $\hbar\mathbf{k}$ is the crystal momentum, and $\hbar$ the Planck constant divided by 2π.

The energy-transport model obtained for silicon semiconductor in [4, 5], starting from the hydrodynamical model based on the maximum entropy principle [2, 3], is given by the following set of balance equations for the electron density n and energy W, coupled to the Poisson equation for the electric potential ϕ

$$\frac{\partial n}{\partial t} + \mathrm{div}(n\mathbf{V}) = 0, \tag{2}$$

$$\frac{\partial (nW)}{\partial t} + \mathrm{div}(n\mathbf{S}) - ne\mathbf{V}\cdot\nabla\phi = nC_W, \tag{3}$$

$$\epsilon\Delta\phi = -e(N_D - N_A - n). \tag{4}$$

where N_D and N_A are the donor and acceptor densities respectively, e is the elementary charge, ϵ is the dielectric constant while div, ∇ and Δ are the divergence, gradient and laplacian operators.

The evolution equations are closed with the constitutive relations for the velocity $\mathbf{V}$ and the energy-flux $\mathbf{S}$

$$\mathbf{V} = D_{11}(W)\nabla\log n + D_{12}(W)\nabla W + D_{13}(W)\nabla\phi, \tag{5}$$

$$\mathbf{S} = D_{21}(W)\nabla\log n + D_{22}(W)\nabla W + D_{23}(W)\nabla\phi. \tag{6}$$

The elements of the diffusion matrix $D = (D_{ij})$ read

$$D_{11} = \frac{c_{22}U^{(0)} - c_{12}F^{(0)}}{c_{11}c_{22} - c_{12}c_{21}}, \quad D_{12} = \frac{c_{22}U^{(0)\prime} - c_{12}F^{(0)\prime}}{c_{11}c_{22} - c_{12}c_{21}},$$

$$D_{13} = -e\frac{c_{22} - c_{12}G^{(0)}}{c_{11}c_{22} - c_{12}c_{21}},$$

$$D_{21} = \frac{c_{11}F^{(0)} - c_{21}U^{(0)}}{c_{11}c_{22} - c_{12}c_{21}}, \quad D_{22} = \frac{c_{11}F^{(0)\prime} - c_{21}U^{(0)\prime}}{c_{11}c_{22} - c_{12}c_{21}},$$

$$D_{23} = e\frac{c_{21} - c_{11}G^{(0)}}{c_{11}c_{22} - c_{12}c_{21}}.$$

All the coefficients c_{ij} and the functions $U^{(0)}$, $F^{(0)}$, $G^{(0)}$ depend on the energy W. The prime denotes derivative with respect to W.

The energy production term has a relaxation form $C_W = -\frac{W-W_0}{\tau_W}$ where τ_W is the energy relaxation time, which depends also on W, and $W_0 = 3/2 k_B T_L$ is the energy at equilibrium, with T_L the lattice temperature, here assumed to be constant.

The expressions of $U^{(0)}$, $F^{(0)}$,$G^{(0)}$, τ_W, c_{ij}, D_{ij} have been obtained in [2, 3] both for parabolic band and Kane's dispersion relation.

However in the case that the conduction energy bands of electrons are described by the Kane dispersion relation, the expressions of $U^{(0)}$, $F^{(0)}$,$G^{(0)}$ τ_W, c_{ij}, D_{ij} require a numerical evaluation of some integrals and for them an analytical expression is not available. Instead in the parabolic band case

$$W = \frac{3}{2} k_B T_n \, ,$$

with T_n electron temperature, and all the constitutive relations have analytical expressions. In particular the fluxes read

$$U^{(0)} = \frac{2}{3} W, \quad m^* F^{(0)} = \frac{10}{9} W^2, \quad m^* G^{(0)} = \frac{5}{3} W, \tag{7}$$

with m^* effective electron mass, while the coefficient c_{ij} can be written as

$$c_{ij}(W) = a_{i1}(W) b_{1j}(W) + a_{i2}(W) b_{2j}(W) \, , \tag{8}$$

where

$$b_{11} = -\frac{21 m^*}{4W}, \qquad b_{12} = b_{21} = \frac{9 m^*}{4W^2}, \qquad b_{22} = -\frac{27 m^*}{20 W^3} \, . \tag{9}$$

The coefficients a_{ij}'s contain the contributions of the various scattering mechanism. If we neglect the impurity scattering, then the a_{ij}'s are the sum of a term due to the acoustic phonon scattering and a term due to the non-polar optical scattering

$$a_{ij} = a_{ij}^{(ac)} + a_{ij}^{(np)} \, .$$

For the acoustic phonon scattering one finds

$$a_{11}^{(ac)} = \frac{32}{3} \frac{\sqrt{2\pi} K_{ac}}{\hbar^3} (m^*)^{3/2} \left(\frac{2}{3} W \right)^{3/2}, \tag{10}$$

$$a_{12}^{(ac)} = 32 \frac{\sqrt{2\pi} K_{ac}}{\hbar^3} (m^*)^{3/2} \left(\frac{2}{3} W \right)^{5/2}, \tag{11}$$

$$a_{21}^{(ac)} = \frac{a_{12}^{(ac)}}{m^*}, \tag{12}$$

$$a_{22}^{(ac)} = 128 \frac{\sqrt{2\pi m^*} K_{ac}}{\hbar^3} \left(\frac{2}{3} W \right)^{7/2} . \tag{13}$$

$K_{ac} = \frac{k_B T_L \Xi_d^2}{4\pi^2 \hbar \rho v_s^2}$ is a physical parameter (see tables 1, 2). Concerning the non polar optical phonon scattering, by assuming that the carrier population is made by the electrons in the six equivalent X-valley [14], one has several contributions because the scattering can be intravalley (that is the electron remain in the same valley) or intervalley (that is the electron are scattered

m_e	electron rest mass	9.1095×10^{-28} g
m^*	effective electron mass	$0.32\ m_e$
T_L	lattice temperature	300^o K
ρ_0	density	2.33 g/cm^3
v_s	longitudinal sound speed	9.18×10^5 cm/sec
Ξ_d	acoustic-phonon deformation potential	9 eV
ϵ_r	relative dielectric constant	11.7
ϵ_0	vacuum dieletric constant	8.85×10^{-18} C/V μm

Table 1: Values of the physical parameters used for silicon

A	Z_f	$\hbar\omega$ (meV)	$D_tK(10^8eV/cm)$
1	1	12	0.5
2	1	18.5	0.8
3	4	19.0	0.3
4	4	47.4	2.0
5	1	61.2	11
6	4	59.0	2.0

Table 2: Coupling constants and phonon energies for the inelastic scatterings in silicon

into another valley)

$$a_{11}^{(np)} = \sum_{A=1}^{6} \frac{4}{3}\left(\frac{2}{3}W\right)^{-1/2} \frac{\sqrt{2\pi}(m^*)^{3/2}(\hbar\omega_{np(A)})^2}{\hbar^3} Z_A K_{np(A)} \sum_{\pm}\left(n_B + \frac{1}{2} \mp \frac{1}{2}\right) e^{\pm\zeta_A} \times \left[K_2(\zeta_A) \mp K_1(\zeta_A)\right], \tag{14}$$

$$a_{12}^{(np)} = \sum_{A=1}^{6} \frac{4}{3}\sqrt{\frac{2}{3}W} \frac{\sqrt{2\pi}(m^*)^{3/2}(\hbar\omega_{np(A)})^2}{\hbar^3} Z_A K_{np(A)} \sum_{\pm}\left(n_B + \frac{1}{2} \mp \frac{1}{2}\right) e^{\pm\zeta_A} \times \left\{3K_2(\zeta_A) + 2\zeta_A\left[K_1(\zeta_A) \mp K_2(\zeta_A)\right]\right\}, \tag{15}$$

$$a_{21}^{(np)} = \frac{a_{12}^{(np)}}{m^*}, \tag{16}$$

$$a_{22}^{(np)} = \frac{4}{3}\left(\frac{2}{3}W\right)^{3/2} \frac{\sqrt{2\pi m^*}(\hbar\omega_{np(A)})^2}{\hbar^3} Z_A K_{np(A)} \sum_{\pm}\left(n_B + \frac{1}{2} \mp \frac{1}{2}\right) e^{\pm\zeta_A} \times \left[K_2(\zeta_A)\left(12 \mp 9\zeta_A + 4\zeta_A^2\right) + K_1(\zeta_A)\left(3\zeta_A \mp 4\zeta_A^2\right)\right], \tag{17}$$

with $\zeta_A = 3\hbar\omega_{np(A)}/(4W)$ and K_i Bessel functions of second kind. A is the valley index. The physical constants appearing in the coefficients are reported in tables 1,2.

MESFET devices are unipolar. On the contrary, MOSFET devices are bipolar and therefore we need a transport model for the holes. Since the contribution of holes to the total current is marginal, it suffices to use a drift-diffusion model. It reads:

$$\frac{\partial p}{\partial t} + \nabla \cdot \mathbf{J_p} = 0\,, \tag{18}$$

$$\mathbf{J_p} = -\mu_p p \nabla\phi - D_p \nabla p \,, \tag{19}$$

where p is the hole density, $\mathbf{J_p}$ is the hole particle flux, μ_p the hole mobility and D_p the diffusivity. In the bipolar case the Poisson equation must include both densities of electrons and holes and reads

$$\mathbf{E} = -\nabla\phi, \qquad \nabla\cdot(\epsilon\nabla\phi) = -e(N_D - N_A - n + p) \,. \tag{20}$$

In order to use the numerical method we will show in the following sections, the MEP Energy-Transport model must be formulated in an equivalent form. This is done in the next section in the parabolic band approximation.

3 Formulation of the model in the framework of linear irreversible thermodynamics

Let us start briefly recalling the basic formulation of linear irreversible thermodynamics. Let $s_n = s_n(u_n, n)$ be the electron system entropy density (where u_n is the electron energy density and n the electron density) and T_n the electron temperature (the lattice and the electron system are assumed to be at different temperature). The first principle of thermodynamics gives:

$$T_n ds_n = du_n - \nu_n dn \,, \tag{21}$$

where ν_n can be interpreted as the chemical potential. Remembering that ϕ is the electrostatic potential, it is convenient to introduce the electrochemical potential $\hat{\phi}_n$ by

$$\hat{\phi}_n = -\nu_n + e\phi \,, \tag{22}$$

In standard irreversible thermodynamics [15] the entropy fluxes J_L^s of the lattice and of the electron system J_n^s are related to the particle and energy fluxes by the following relationships:

$$\mathbf{J_L^s} = \frac{\mathbf{J_L^u}}{T_L}, \quad \mathbf{J_n^s} = \frac{\mathbf{J_n^u} - \nu_n \mathbf{J_n}}{T_N} \,, \tag{23}$$

where $\mathbf{J_L^u}$ and $\mathbf{J_n^u}$ are the lattice and electron energy flux respectively, $\mathbf{J_n}$ the electron particle flux, T_L and T_n the lattice and electron gas temperature respectively. Now, according to the tenets of linear irreversible thermodynamics [15] the thermodynamic forces are linearly related to the thermodynamic fluxes as follows:

$$\mathbf{J_n} = \frac{L_{11}}{T_n}\nabla\hat{\phi}_n + L_{12}\nabla\frac{1}{T_n} \,, \tag{24}$$

$$T_n\mathbf{J_n^s} = \frac{L_{21}}{T_n}\nabla\hat{\phi}_n + L_{22}\nabla\frac{1}{T_n} \,, \tag{25}$$

where the matrix L_{ij} is symmetric as a consequence of the Onsager reciprocity relations. In terms of electron energy flux $\mathbf{J_u^s}$ one rewrites the above equations as

$$\mathbf{J_n} = \frac{L_{11}}{T_n}\nabla\hat{\phi}_n + L_{12}\nabla\frac{1}{T_n}, \tag{26}$$

$$\mathbf{J_n^u} = \Big(\nu_n\frac{L_{11}}{T_n} + \frac{L_{21}}{T_n}\Big)\nabla\hat{\phi}_n + (\nu_n L_{12} + L_{22})\nabla\frac{1}{T_n} \,. \tag{27}$$

Now, for the electron system, described by a probability density function f, the entropy density in the maxwellian limit of the Fermi-Dirac statistics is defined as

$$s_n = -k_B \int_B (f \log f - f) d^3\mathbf{k} \,, \tag{28}$$

where $\mathbf{k}$ is the electron wave-vector which belongs to the first Brillouin zone. This latter in the parabolic band approximation is extended to all $\mathbf{R^3}$.

By introducing the function

$$\eta(f) = -k_B(f \log f - f) \,,$$

we can write

$$s_n = \int_B \eta(f) d^3\mathbf{k} \,. \tag{29}$$

The zeroth order maximum entropy distribution function, as shown in [2, 3] is

$$f_{ME} = \exp\left(-\frac{\lambda}{k_B} - \lambda^W \mathcal{E}\right) \,, \tag{30}$$

where λ,λ^W are the Langrange multipliers relative to the density and energy. It follows that

$$\eta(f_{ME}) = k_B f_{ME} \left(1 + \frac{\lambda}{k_B} + \lambda^W \mathcal{E}\right). \tag{31}$$

Since

$$df_{ME} = -f_{ME} \left(\frac{d\lambda}{k_B} + \mathcal{E} d\lambda^W\right) \,, \tag{32}$$

it follows

$$d\eta = -f_{ME} \left[\left(\frac{\lambda}{k_B} + \mathcal{E}\lambda^W\right)(d\lambda + k_B \mathcal{E} d\lambda^W)\right] \,. \tag{33}$$

Consequently, for the differential of the entropy density, ds_n, we have

$$ds_n = \int_B d\eta d^3\mathbf{k} = -\frac{\lambda}{k_B} n d\lambda - d(\lambda\lambda^W) u_n - k_B \lambda^W d\lambda^W Z \,, \tag{34}$$

where n is the electron particle density calculated with the zeroth order f_{ME} distribution function, which reads

$$n = \int_B f_{ME} d^3\mathbf{k}.$$

Likewise u_n is the electron energy density calculated with the zeroth order f_{ME} distribution function and reads

$$u_n = nW = \int_B \mathcal{E} f_{ME} d^3\mathbf{k} \,,$$

while Z is the quantity

$$Z = \int_B \mathcal{E}^2 f_{ME} d^3\mathbf{k}.$$

From the definition of n, after some standard computation, we have

$$dn = -n\frac{d\lambda}{k_B} - d\lambda^W u_n \,. \tag{35}$$

Likewise, from the definition of u_n we get

$$du_n = -u_n\frac{d\lambda}{k_B} - d\lambda^W Z. \tag{36}$$

Now, from (32)-(34), we easily get

$$ds_n = \lambda dn + k_B\lambda^W du_n \,, \tag{37}$$

which has the same form as equation (18) provided the following identifications are made

$$k_B\lambda^W = \frac{1}{T_n}, \quad \nu_n = -\lambda T_n. \tag{38}$$

Therefore, until now, we have proved that the expression for the entropy differential as obtained from the maximum entropy ansatz can be written in the form of linear irreversible thermodynamics.

In terms of $W = \frac{u_n}{n}$, the energy per particle, we can write equation (35) as

$$\frac{dn}{n} = -\frac{d\lambda}{k_B} - W d\lambda^W \,. \tag{39}$$

Then we can introduce the primitive (defined up to a constant)

$$F(W) = \int W\frac{d\lambda^W}{dW}dW \,,$$

and integrate (39) obtaining

$$\lambda = -k_B \log n - k_B F(W) \,, \tag{40}$$

which, after substituting into the equation (38), yields

$$\nu_n = k_B T_n \log n + k_B T_n F(W), \tag{41}$$

$$d\nu_n = k_B T_n d\log n + \big(k_B \log n + k_B F - \frac{W}{T_n}\big)dT_n \,. \tag{42}$$

Substituting into equations (26),(27) yields

$$\mathbf{J_n} = -L_{11}k_B\nabla\log n + \frac{qL_{11}}{T_n}\nabla\phi - \left[\frac{L_{11}}{T_n}\left(k_B\log n + k_B F - \frac{W}{T_n}\right) + \frac{L_{12}}{T_n^2}\right]\nabla T_n \,, \tag{43}$$

$$\mathbf{J_n^u} = -(\nu_n L_{11} + L_{21})k_B\nabla\log n + (\nu_n L_{11} + L_{21})\frac{e}{T_n}\nabla\phi - \tag{44}$$

$$\left[\left(\frac{\nu_n L_{11} + L_{21}}{T_n}\right)\left(k_B\log n + k_B F - \frac{W}{T_n}\right) + \left(\frac{\nu_n L_{12} + L_{22}}{T_n^2}\right)\right]\nabla T_n. \tag{45}$$

By comparing with the maximum entropy derived constitutive equations for the energy transport model (5)-(6) we have the following identification

$$D_{11} = -\frac{k_B L_{11}}{n}, \quad D_{13} = \frac{eL_{11}}{nT_n}, \tag{46}$$

$$D_{12} = -\frac{1}{n}\left[\frac{L_{11}}{T_n}\left(k_B \log n + k_B F - \frac{W}{T_n}\right) + \frac{L_{12}}{T_n^2}\right]\frac{dT_n}{dW}, \tag{47}$$

$$D_{21} = -\frac{k_B(\nu_n L_{11} + L_{21})}{n}, \quad D_{23} = e\frac{\nu_n L_{11} + L_{21}}{nT_n}, \tag{48}$$

$$D_{22} = -\frac{1}{n}\left[\frac{\nu_n L_{11} + L_{21}}{T_n}\left(k_B \log n + k_B F - \frac{W}{T_n}\right) + \frac{\nu_n L_{12} + L_{22}}{T_n^2}\right]\frac{dT_n}{dW}, \tag{49}$$

from which we get, after some standard algebra,

$$L_{11} = -\frac{nD_{11}}{k_B}, \tag{50}$$

$$L_{12} = -\frac{3}{2}nk_B T_n^2 D_{12} + nD_{11}T_n\left(\log\frac{n}{N_c} - \frac{3}{2}\right), \tag{51}$$

$$L_{22} = -\frac{3}{2}nk_B T_n^2 D_{22} + \nu_n T_n n D_{11}\left(\log\frac{n}{N_c} - \frac{3}{2}\right) - L_{12}\left[k_B T_n\left(\log\frac{n}{N_c} - \frac{3}{2}\right) + \nu_n\right], \tag{52}$$

where we have used the following results

$$\log n + F = \log\frac{n}{N_c}, \quad \frac{W}{T_n} = \frac{3}{2}k_B\,,$$

with

$$N_c = 2\left(\frac{2\pi k_B m^* T_n}{\hbar^2}\right)^{\frac{3}{2}}, \quad n = N_c(T_n)\exp\left(e\frac{\phi + \varphi_n}{k_B T_n}\right),$$

where φ_n is the so-called electron quasi-Fermi level. At this point we want to transform, in the stationary case, the system (2)-(4) in the following form

$$-\text{div}\ \mathbf{J_n} = 0, \tag{53}$$

$$-\text{div}\ \mathbf{J_n^T} + \frac{3}{2}k_B n\frac{T_n - T_0}{\tau_W} = 0, \tag{54}$$

$$\text{div}\ \mathbf{D} = e(N_D - N_A - n + p), \tag{55}$$

$$\mathbf{J_n} = A_{11}\nabla\left(\frac{\varphi_n}{T_n}\right) + A_{12}\nabla\left(\frac{-1}{T_n}\right), \tag{56}$$

$$\mathbf{J_n^T} = A_{21}\nabla\left(\frac{\varphi_n}{T_n}\right) + A_{22}\nabla\left(\frac{-1}{T_n}\right)\,, \tag{57}$$

where $\mathbf{D}$ is the electric displacement vector and, for the sake of simplicity in the notation, we denote now with $\mathbf{J_n}$ the electron current $-en\mathbf{J_n}$. The generation-recombination effects have been neglected. In order to get the sought transformation we need to find the analytical expression of the coefficients A_{ij} as functions of the variables D_{ij}. Let us start by finding the coefficients A_{11} and A_{12}. First of all, we note that

$$\mathbf{J_n} = -en\mathbf{V} = -en\left[D_{11}\nabla\log n + D_{12}\nabla W + D_{13}\nabla\phi\right]\,. \tag{58}$$

After some algebra we get the following results

$$A_{11} = e^2 L_{11}, \quad A_{12} = -e^2 L_{11}\phi - en\left\{\frac{3}{2}D_{11}T_n + \frac{3}{2}k_B T_n^2 D_{12}\right\} . \tag{59}$$

Likewise, noting that

$$\mathbf{J_n^T} = -\mathbf{J_n^u} - \phi \mathbf{J_n} , \tag{60}$$

we get

$$A_{21} = e^2 L_{11}\varphi_n + eL_{21}, \quad A_{22} = e^2 L_{11}\varphi_n^2 + 2eL_{21}\varphi_n + L_{22}. \tag{61}$$

We end this section with the remark that a similar transformation is not known for a non-parabolic band. The point is that as consequence of relations (46) one has

$$D_{11} = -\frac{k_B T_n}{e} D_{13} ,$$

that is *the Einstein relation must always hold even far from equilibrium.* This property is satisfied by the parabolic model while for the Kane dispersion relation is valid only close to equilibrium [16].

4 The Numerical Approach

The MEP energy-transport model given as in (53)-(57) has the same structure as the family of models studied in [7]. In the last reference, the diffusion matrix A which depends on parameters β,c,γ, is given explicitly by

$$A_{11} = n\mu_n e T_n , \tag{62}$$

$$A_{12} = n\mu_n e T_n \left(\beta \frac{k_B T_n}{e}\gamma - \varphi_n + \chi\right) , \tag{63}$$

$$A_{21} = A_{12} , \tag{64}$$

$$A_{22} = n\mu_n e T_n \left[\left(\beta \frac{k_B T_n}{e}\gamma - \varphi_n + \chi\right)^2 + (\beta - c)\left(\frac{k_B T_n}{e}\right)^2\right] , \tag{65}$$

and by an appropriate choice of the parameters, the Stratton Energy-Transport model or the Degond Energy-Transport model can be recovered as well as some simplified hydrodynamical models (SHD). [13, 9]

In the present paper the numerical scheme developed in [7] has been adapted in order to take into account the expression of the diffusion matrix for the MEP model.

Let us recall some key features of the numerical scheme used.

- Mixed finite element approximation (the classical Raviart-Thomas RT_0 is used for space discretization, see [7, 8, 17] for more details).
- Operator-splitting techniques for solving saddle point problems arising from mixed finite elements formulation [18].
- Implicit scheme (backward Euler) for time discretization of the artificial transient problems generated by operator splitting techniques.

- A block-relaxation technique, at each time step, is implemented in order to reduce as much as possible the size of the successive problems we have to solve, by keeping at the same time a large amount of the implicit character of the scheme.
- Each non-linear problem coming from relaxation technique is solved via the Newton-Raphson method.

Concerning the block relaxation technique, three main steps have to be considered

- A step related to the Poisson equation for the computation of φ^{k+1} and $\mathbf{D}^{k+1}$ (the other unknowns, frozen at the last known values, i.e. φ_p^k,$\mathbf{J}_p^k$,φ_n^k,$\mathbf{J}_n^k$,T_n^k,$\mathbf{J}_{T_n}^k$)
- A second step related to the hole continuity equation (if needed) for the computation of φ_p^{k+1} and $\mathbf{J}_p^{k+1}$
- A third step in which the variables φ_n^{k+1},$\mathbf{J}_n^{k+1}$,T_n^{k+1}, $\mathbf{J}_{T_n}^{k+1}$ are computed simultaneously.

The reason of such a procedure are explained in [7] and are essentially due to a stronger physical coupling between equation relative to electron continuity and electron temperature.

Let us detail, now, the problem we have to solve during the third step of the relaxation process. We denote by Ω the integration domain with boundary $\Gamma_N \cup \Gamma_D$, with Γ_N and Γ_D the parts of boundary where Newmann and Dirichlet condition are imposed.

- We have to find

$$\mathbf{U^{k+1}} = \begin{pmatrix} U_1^{k+1} \\ U_2^{k+1} \end{pmatrix} = \begin{pmatrix} \frac{\varphi_n^{k+1}}{T_n} \\ -\frac{1}{T_n} \end{pmatrix} : \Omega \longrightarrow \mathbf{R^q}$$

and

$$\mathbf{J}^{k+1} = \begin{pmatrix} \mathbf{J}_n^{k+1} \\ \mathbf{J_{T_n}} \end{pmatrix} = \begin{pmatrix} \mathbf{J}_1^{k+1} \\ \mathbf{J}_2^{k+1} \end{pmatrix} : \Omega \longrightarrow \left[\mathbf{R^d}\right]^q$$

such that :

$$\begin{aligned} &S_{i,j}^k(\mathbf{x})\frac{U_j^{k+1}-U_j^k}{\Delta t} - \mathrm{div}(\mathbf{J}_i^{k+1}) + F_i(\mathbf{x},\mathbf{U}^{k+1}) = 0, \qquad i = 1,\ldots,q=2, \\ &\mathbf{J}_i^{k+1} = A_{i,j}(\mathbf{x},\mathbf{U}^{k+1})\,\nabla U_j^{k+1}, \quad i = 1,\ldots,q=2. \end{aligned} \tag{66}$$

with the boundary conditions:

$$U_i^{k+1} = G_i(x) \text{ on } \Gamma_D \qquad \text{and} \qquad \mathbf{J}_i^{k+1}\cdot\boldsymbol{\nu} = 0 \text{ on } \Gamma_N, \quad i = 1,\ldots,q\,, \tag{67}$$

and where S_{ij}^k is a positive definite matrix which may be chosen (and adapted) by the user. The vector $\boldsymbol{\nu}$ represents the unit external normal to Ω in Γ_N,. If other unknowns of the problem appear in expressions (specially in F_i and A_{ij}) they are considered at previous step k.

The dual mixed variational formulation which allows us the mixed finite element approach needs the introduction of the following functional spaces

$$H(\mathrm{div}) = \{\omega \,|\, \omega \in (L^2(\Omega))^p,\ \mathrm{div}(\omega) \in L^2(\Omega)\},$$
$$V_0 = \{\omega \,|\, \omega \in H(\mathrm{div}), \omega\cdot\mathbf{n} = 0 \text{ on } \Gamma_N\}.$$

and is given by:

Let us find $\left(\mathbf{U}^{k+1}, \mathbf{J}^{k+1}\right) \in [L^2(\Omega)]^q \times [V_0]^q$ such that

$$\int_\Omega V_i \, S^k_{i,j}(\mathbf{x}) \frac{U^{k+1}_j - U^k_j}{\Delta t} dx - \int_\Omega V_i \, \mathrm{div}(\mathbf{J}^{k+1}_i) dx + \int_\Omega V_i \, F_i(\mathbf{x}, \mathbf{U}^{k+1}) dx = 0 \;\; \forall V \in [L^2(\Omega)]^q, \tag{68}$$

$$\int_\Omega B_{i,j}(\mathbf{x}, U^{k+1}) \, \mathbf{W}_i \cdot \mathbf{J}^{k+1}_j dx + \int_\Omega \mathrm{div}(\mathbf{W}_i) \, U^{k+1}_i dx - \int_{\Gamma_D} G_i(\mathbf{x}) \, \mathbf{W}_i \cdot \nu d\Gamma = 0 \;\; \forall \mathbf{W} \in [\mathbf{V_0}]^q \,, \tag{69}$$

with

$$B(\mathbf{x}, \mathbf{U}^{k+1}) = [A(\mathbf{x}, \mathbf{U}^{k+1})]^{-1}.$$

The finite element formulation is obtained by replacing the spaces $L^2(\Omega)$ and V_0 by finite dimensional subspaces generated over a triangulation $\mathcal{T}_h$ of Ω using Raviart-Thomas RT_0 element i.e.

$$L_h = \{v_h \in L^2(\Omega) \;|\; \forall \mathcal{K} \in \mathcal{T}_h, \; v_h|_\mathcal{K} = \mathrm{Const}\},$$

$$V_{0h} = \{\omega_h \in V_0 \;|\; \forall \mathcal{K} \in \mathcal{T}_h, \; \omega_h = \left| \begin{array}{cc} \alpha_\mathcal{K} & \\ \beta_\mathcal{K} & \end{array} + \gamma_\mathcal{K} \right| \begin{array}{c} x \\ y \end{array} \Big\}.$$

where $\alpha_\mathcal{K}$, $\beta_\mathcal{K}$ and $\gamma_\mathcal{K}$ are numerical coefficients [7]. Applying Newton-Raphson method to the discrete version of the system (68), (69) and after the elimination of the primal variable $\mathbf{U}$ we obtain a sequence of linear problems (index l) for the dual variable $\mathbf{J}^{l+1}$ only

$$\begin{aligned} &\int_\Omega B_{i,j}\delta_{j,\beta} \, \mathbf{W}_i \cdot \mathbf{J}^{l+1}_\beta dx + \int_\Omega \Lambda_{\alpha,\beta} \left(\mathrm{div}(\mathbf{W}_i)\delta_{i,\alpha} + \partial_{U_\alpha}(B_{i,j}) \, \mathbf{W}_i \cdot \mathbf{J}^l_j\right) \mathrm{div}(\mathbf{J}^{l+1}_\beta) dx \\ &= \int_\Omega \Lambda_{\alpha,\beta} \left(\mathrm{div}(\mathbf{W}_i)\delta_{i,\alpha} + \partial_{U_\alpha}(B_{i,j}) \, \mathbf{W}_i \cdot \mathbf{J}^l_j\right) \left(S^k_{\beta,\gamma} \frac{U^l_\gamma - U^k_\gamma}{\Delta t} + F_\beta \right) dx \\ &- \int_\Omega \mathrm{div}(\mathbf{W}_i) \, U^l_i dx + \int_{\Gamma_D} G_i \, \mathbf{W}_i \cdot \boldsymbol{\nu} d\Gamma = 0, \qquad\qquad \forall \mathbf{W} \in [V_h]^q \,. \end{aligned} \tag{70}$$

Then the primal variable $\mathbf{U}^{l+1}$ is recovered, element by element, by

$$U^{l+1}_\alpha - U^l_\alpha \big|_\mathcal{K} = -\Lambda_{\alpha,\beta} \left(S^k_{\beta,\gamma} \frac{U^l_\gamma - U^k_\gamma}{\Delta t} + F_\beta(U^l) - \mathrm{div}(\mathbf{J}^{l+1}_\beta) \right) \Big|_\mathcal{K}, \alpha = 1, ..., q = 2, \tag{71}$$

where

$$\left[\Lambda_{\alpha,\beta}(\mathbf{x}, \mathbf{U}^l)\right] = \left[\frac{S^k_{\alpha,\beta}(\mathbf{x})}{\Delta t} + \partial_{U_\beta}(F_\alpha(\mathbf{x}, \mathbf{U}^l)) \right]^{-1}. \tag{72}$$

In order to adapt the numerical scheme to the formulation of the diffusion matrix for the MEP model, we need first the inverse of the matrix A

$$B = A^{-1} \,,$$

and, then, (due to the Newton method) the partial derivatives of the elements of B with respect to the entropy variables ($U_1 = \frac{\varphi_n}{T_n}, U_2 = -\frac{1}{T_n}$) i.e.

$$\frac{\partial B_{ij}}{\partial U_\alpha}, \qquad i,j,\alpha = 1,2\,.$$

In Montarnal's approach, the A_{ij} are given with very simple expressions, so it was relatively easy to find also analytically the matrix B and its partial derivatives. In the present case, the construction of the diffusion matrix A can be summarized as follows

$$C \longrightarrow D \longrightarrow L \longrightarrow A$$

which has to be completed by the step

$$A \longrightarrow B = A^{-1}$$

for algorithmic reasons. It is easy to see that it will be extremely hard (or practically impossible) to express analytically the partial derivatives of B. But, in fact, what we need effectively in the numerical process is a way to evaluate a partial derivative of B_{ij} for a given value of the unknown variables. This can be done more easily by following the rules used in software devoted in automatic differentiation of (FORTRAN) codes, like for example, Odyssée [19]. Each line of code is differentiated with respect to prescribed variables following classical rules of differentiation and function and derivatives are computed simultaneously within the same routine. In this particular application the elements $c_{ij}(T_n)$ of the matrix C have been given on a discrete set of points T_n^i and approximated by cubic splines, in order to recover a C^1 function.

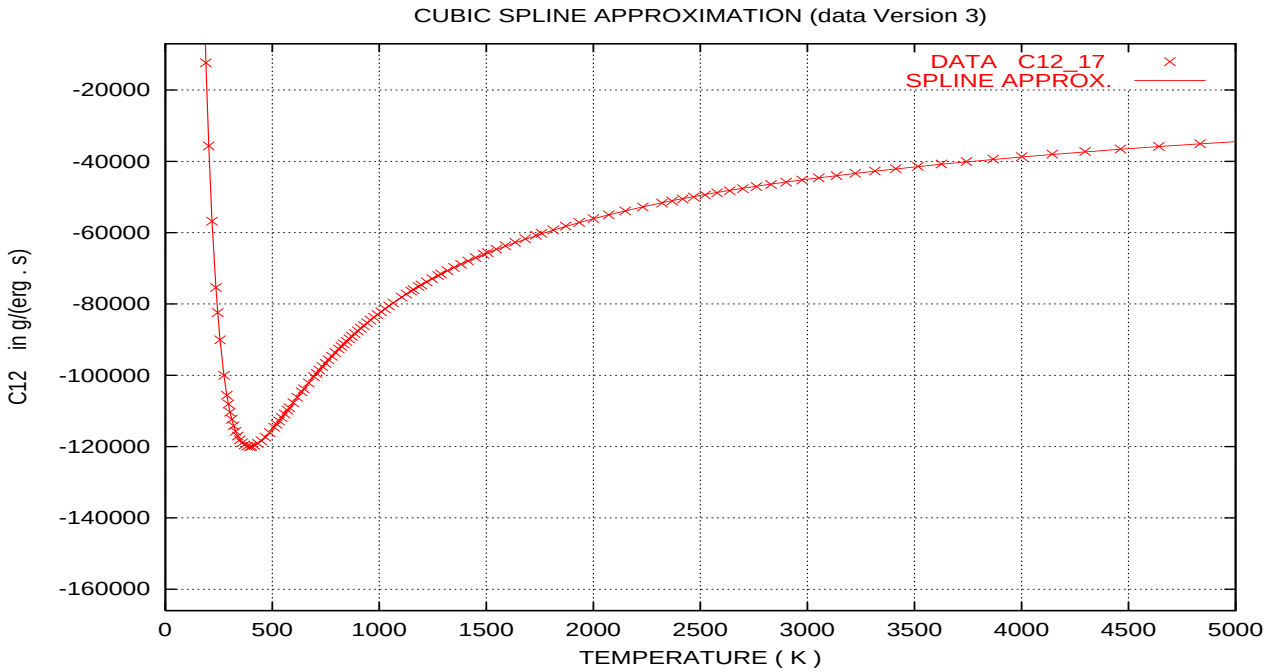

Figure 1: Cubic spline approximation.

See for example figure 1 which gives the result of cubic spline smoothing for the coefficient c_{12}. The cross points are the given data and the continuous line the approximation realized using the *FITPACK* package from P. Dierckx. The relative error is less than 0.1 % at given points.

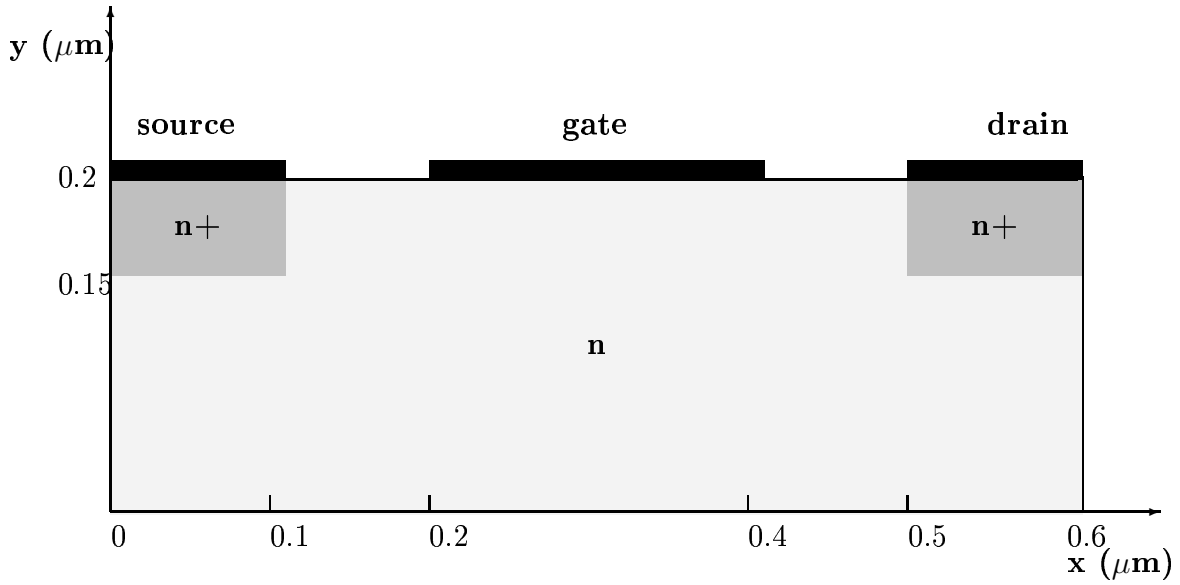

Figure 2: Schematic representation of a bidimensional MESFET

5 Simulation of a 2D silicon MESFET

In this section we check the validity and the efficiency of the numerical method by simulating a bidimensional Metal Semiconductor Field Effect Transistor (MESFET). The shape of the device is taken as rectangular and it is pictured in fig. 2.

The axes of the reference frame are chosen parallel to the edges of the device. We take the dimensions of the MESFET to be such that the numerical domain is

$$\Omega = [0, 0.6] \times [0, 0.2]$$

where the unit length is the micron.

The regions of high doping n^+ are the subset

$$[0, 0.1] \times [0.15, 0.2] \cup [0.5, 0.6] \times [0.15, 0.2].$$

The contacts at the source and drain are 0.1 μm wide and the contact at the gate is 0.2 μm wide. The distance between the gate and the other two contacts is 0.1 μm. The same doping concentration as in [20] is considered

$$n_D(x) - n_A(x) = \begin{cases} 3 \times 10^{17}\text{cm}^{-3} & \text{in the } n^+ \text{ regions} \\ 10^{17}\text{cm}^{-3} & \text{in the } n \text{ region} \end{cases}$$

with abrupt junctions.

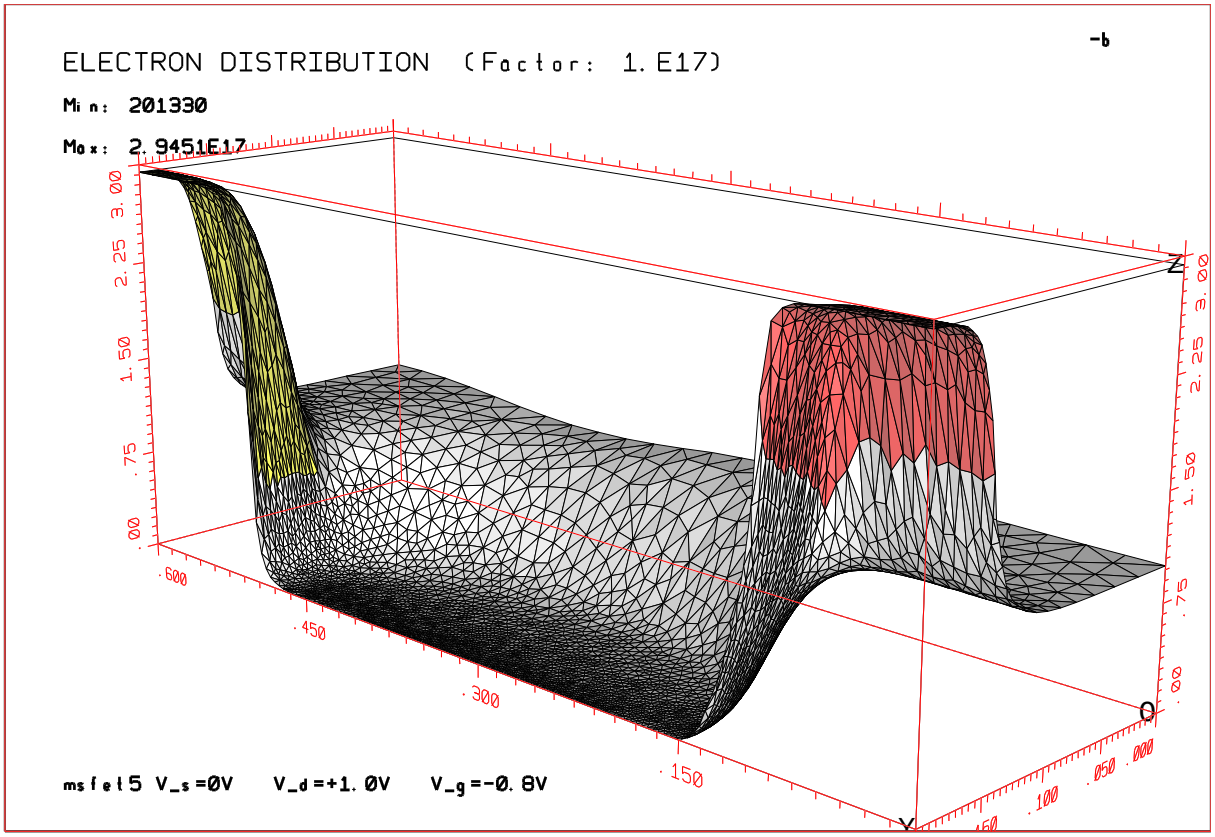

Figure 3: Stationary solution for the electron density in MESFET (cm^{-3}).

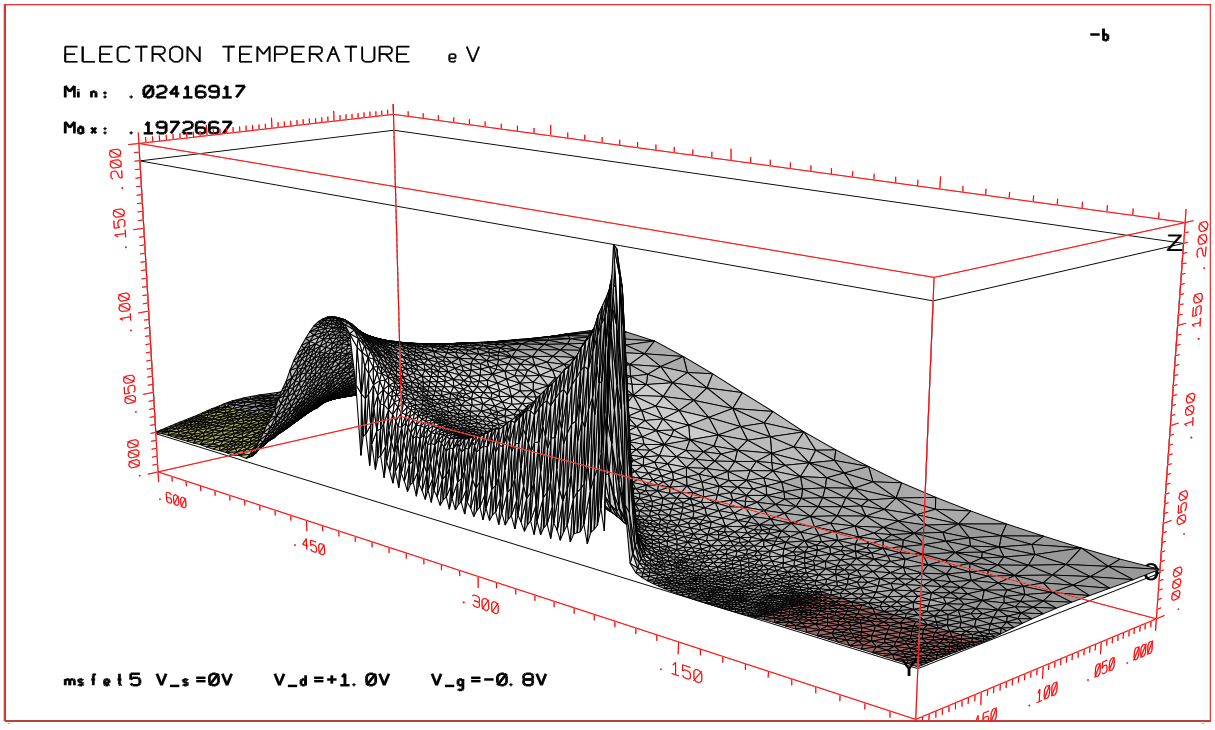

Figure 4: Stationary solution for the electron temperature in MESFET (eV).

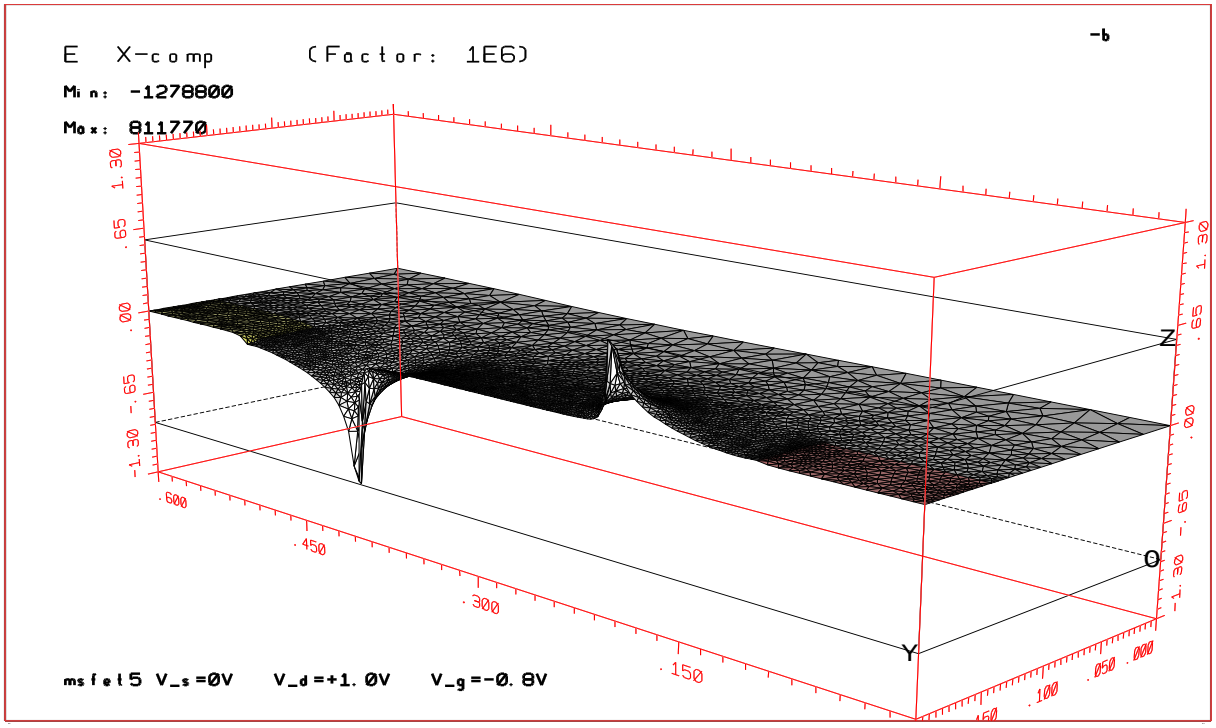

Figure 5: Stationary solution for the x-component of the electric field in MESFET (Volt/cm).

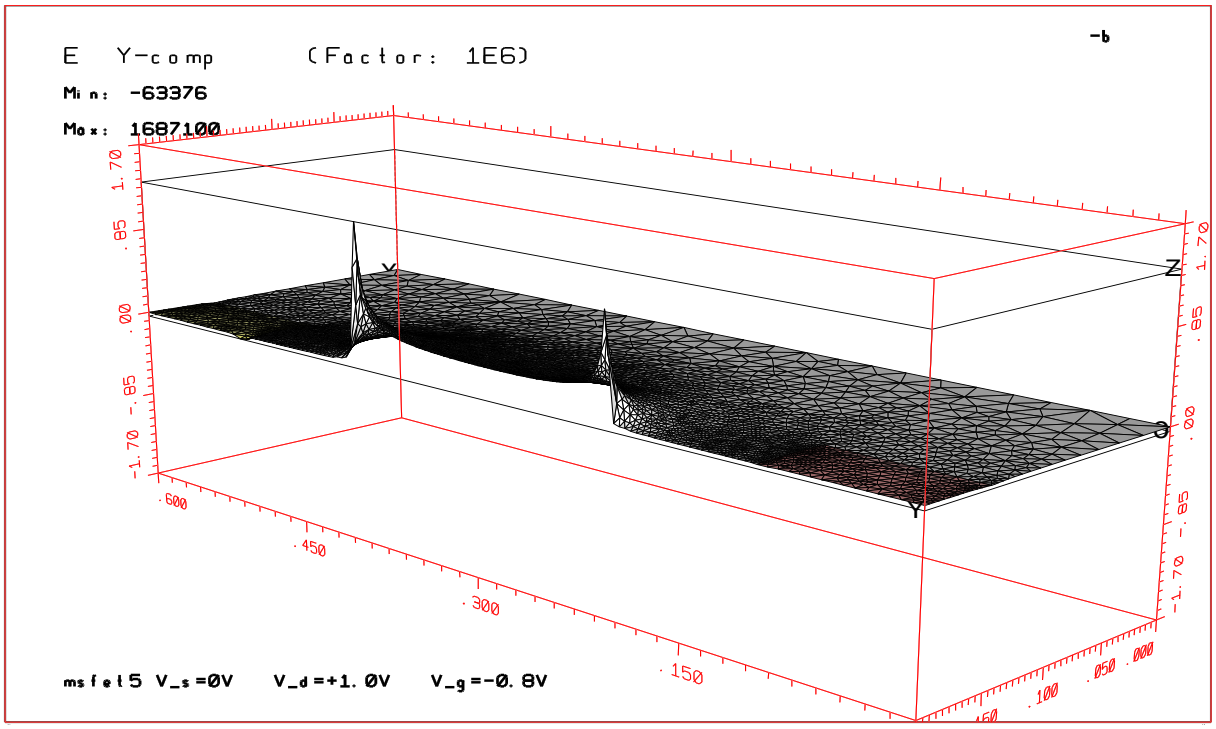

Figure 6: Stationary solution for the y-component of the electric field in MESFET (Volt/cm).

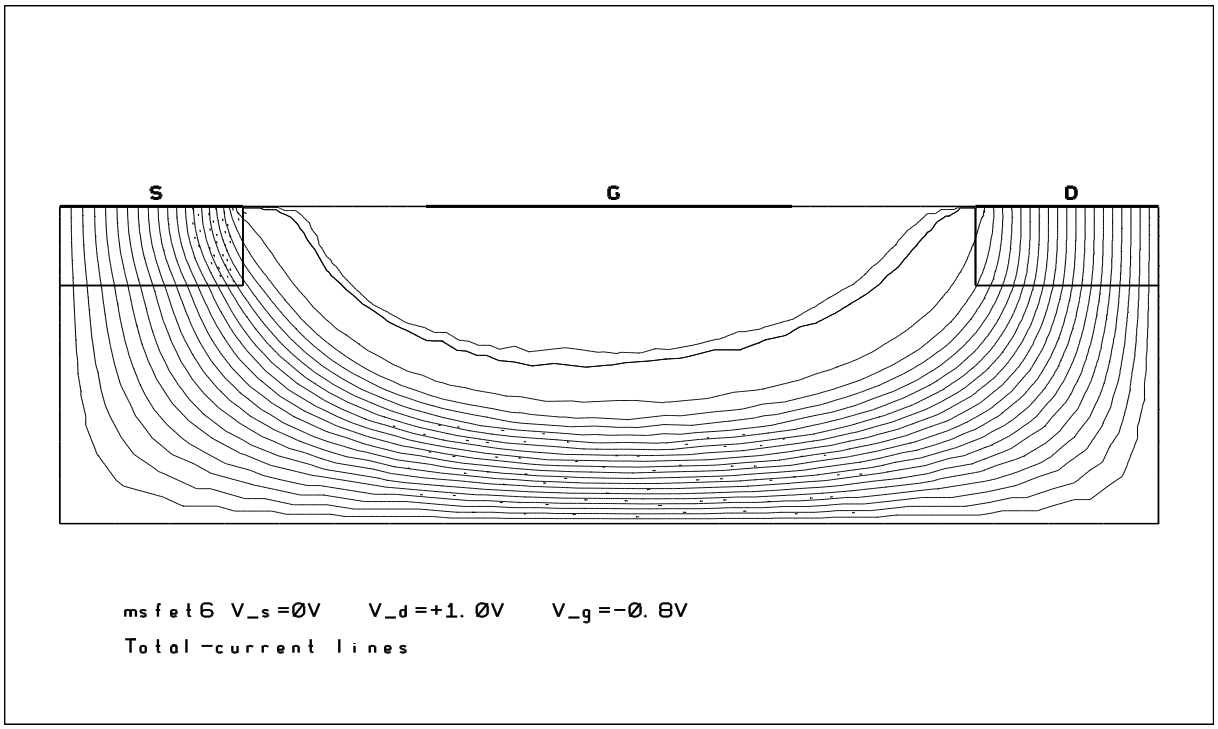

Figure 7: Current lines for the MEP model in MESFET.

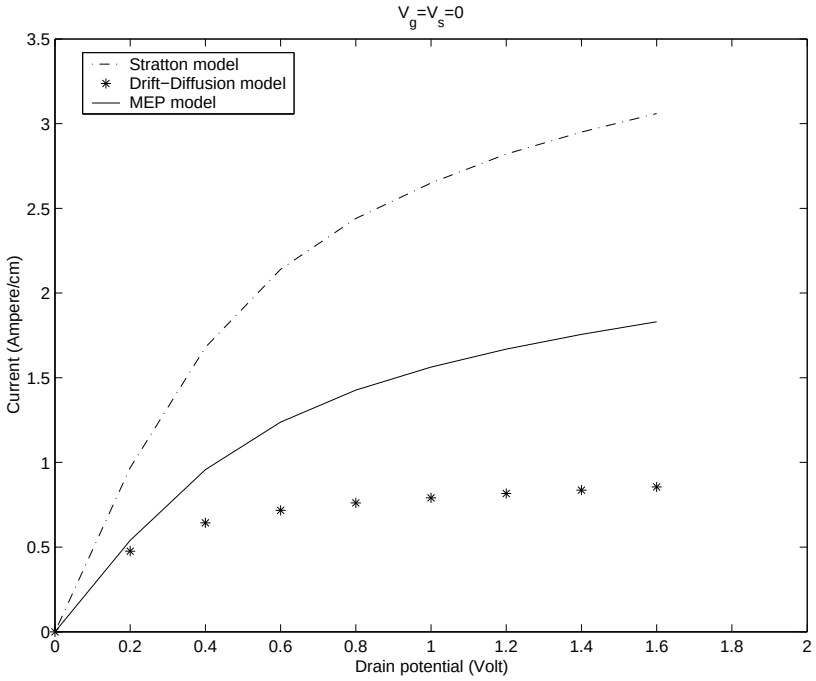

Figure 8: Characteristic curve. $I_S(V_{DS})$ at $V_G = 0$.

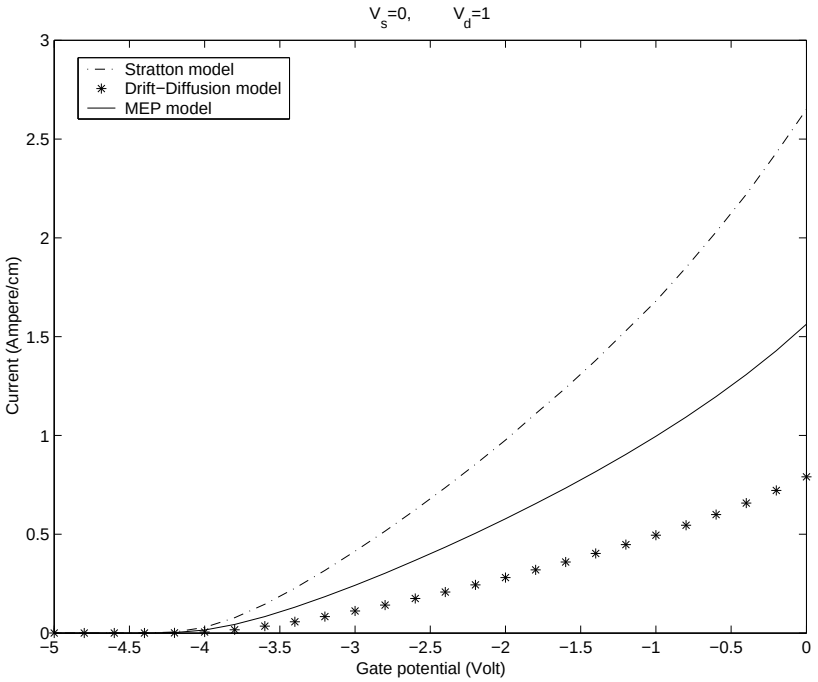

Figure 9: Characteristic curve. $I_S(V_G)$ at $V_{DS} = 1$.

The same device has been simulated, in the nonparabolic band case, in [5] by using a finite difference scheme and by considering the full hydrodynamical model based on MEP [2, 3, 4].

We denote by Γ_D that part of $\partial\Omega$, the boundary of Ω, which represents the source, gate and drain

$$\Gamma_D = \{(x, y) : y = 0.2,\ 0 \le x \le 0.1,\ 0.2 \le x \le 0.4,\ 0.5 \le x \le 0.6\}\,.$$

The other part of $\partial\Omega$ is labelled as Γ_N. The boundary conditions are assigned as follows. We have ohmic contacts in source and drain:

$$\phi = \phi_{int} + V_{app}\,, \tag{73}$$

$$\varphi_n = -V_{app}\,. \tag{74}$$

On the gate we have a Schottky contact

$$\phi = \phi_{int} + V_B + V_{app}\,, \tag{75}$$

$$\varphi_n = -V_{app}\,, \tag{76}$$

where V_B is the barrier potential modelling the Schottky contact [21]. The built in potential ϕ_{int} is the solution of

$$F(\phi_{int}) = e(n(\phi_{int}) - p(\phi_{int}) - N_D + N_A) = 0\,,$$

where the quasi-Fermi level are taken as $\varphi_n = \varphi_p = 0$. The other boundary conditions are

$$W = W_0, \quad \text{on } \Gamma_D, \tag{77}$$

$$\boldsymbol{\nu} \cdot \nabla n = 0, \quad \boldsymbol{\nu} \cdot \nabla W = 0, \quad \boldsymbol{\nu} \cdot \nabla \phi = 0, \quad i = 1, 2 \quad \text{on } \Gamma_N. \tag{78}$$

Here ∇ is the bidimensional gradient operator while $\boldsymbol{\nu}$ is the unit outward normal vector to $\partial\Omega$ in the considered points. For the numerical simulation we start from the equilibrium state ($V_{app} = 0$) and after a desired bias point is reached by following a path in the space of applied potential (via potential increments). First we follow the path $V_S = 0$,$V_G = 0$ and $V_D = 0$ to 1.6 Volt by step of 0.2 Volt an after starting from the point $V_S = 0$,$V_G = 0$ and $V_D = 1$ we decrease the gate potential V_G from 0 to -5 Volt by step of 0.2 Volt. When the gate potential is sufficiently low, no ("significant") current flow from drain to source.

The results are shown in figure [3]-[9]. The qualitative behavior is similar to that obtained in [5], but the maximum values for energy and velocity are higher because here the parabolic band approximation has been used.

6 Simulation of a 2D silicon MOSFET

In this section we check the validity of our energy-transport model and the efficiency of the numerical method by simulating a bidimensional metal oxide semiconductor field effect transistor (MOSFET). The shape of the device is pictured in Figure 10. The axes of reference

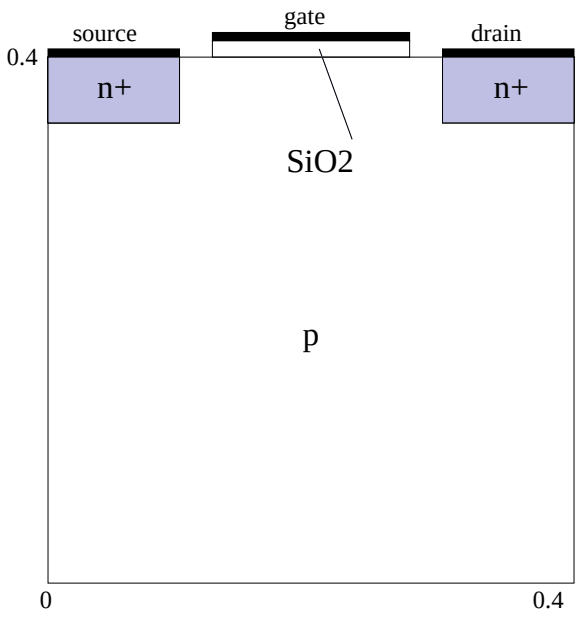

Figure 10: Schematic representation of a bidimensional MOSFET.

frame are chosen parallel to the edges of the device. We take the dimensions of the silicon part of the MOSFET to be such that the numerical domain is

$$[0, 0.4] \times [0, 0.4]$$

and at the top of the silicon part the silicon oxide domain is

$$[0.125, 0.275] \times [0.4, 0.406]$$

where the length is the micron.

The regions of high-doping n^+ are the subset

$$[0, 0.1] \times [0.35, 0.4] \cup [0.3, 0.4] \times [0.35, 0.4].$$

The contacts at the source and drain are $0.1\mu m$ wide and the contact at the gate is $0.15\mu m$ wide. The distance between the gate and the other two contacts is $0.025\mu m$. A grid of 4644 elements has been used (see figure 11): 3344 in the bulk zone, 343 in the n^+ source zone, 357 in the n^+ drain zone and 600 in the oxide zone. The doping concentration is

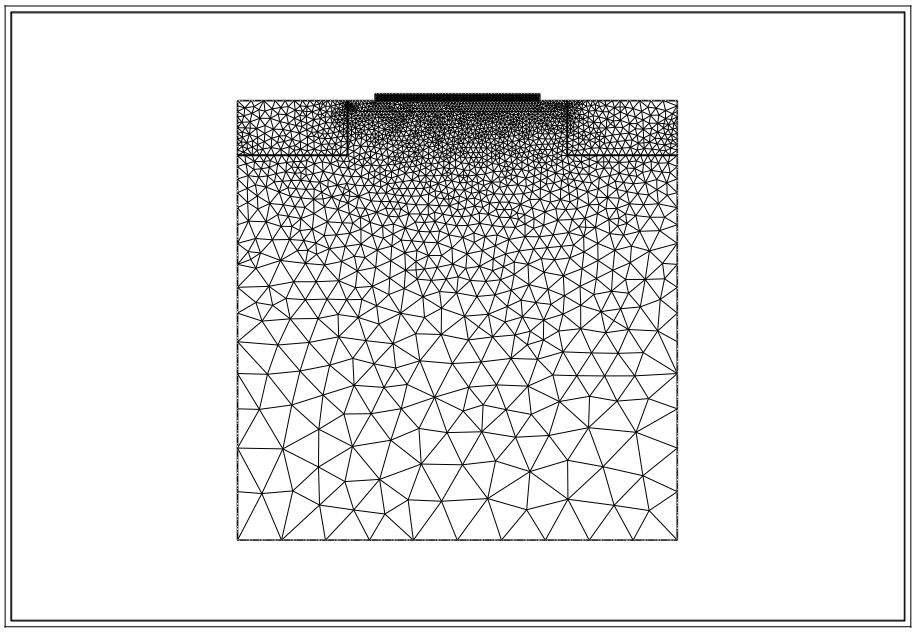

Figure 11: Mesh used for the computation.

$$n_D(x) - n_A(x) = \begin{cases} 10^{18} cm^{-3} \text{in the } n^+ \text{ regions} \\ -10^{14} cm^{-3} \text{in the } p \text{ region} \end{cases}$$

with abrupt junctions.

We have assumed ohmic contacts on the source, drain and gate and Schottky contact on the bulk. Moreover, we have assumed homogeneous Neumann conditions on the remaining part of the boundary. In order to reach the desired bias, $V_d = 1.0$ $V_s = 0$ and $V_g = 0.5$, we first compute the equilibrium state and then the previous point is reached by continuation on applied potential. First, we go to $V_d = 1.0$ by steps of 0.1 Volt and after we go to $V_g = 0.5$ within two steps of 0.25 Volt. The total amount of computational time to reach the desired bias ($V_d = 1$, $V_s = 0$, $V_g = 0.5$, using the mesh given on figure 11) was about 40' on a laptop computer (COMPAQ M700, 1 Ghz, RAM=384 Mb, running Linux).

In order to estimate how much fine the mesh should be, we have compared the source current for different meshes. The results are summarized in table 3. There are not relevant differences among the results with meshes 3, 4 and 5. Therefore we use in the simulations the mesh 3 of the table because less time expensive.

The results of the numerical integration are reported in figures (12)-(19). For the sake of completeness we have also compared the current lines obtained with the Stratton model with those given by the MEP model (figures 17 and 18). The qualitative behaviour is almost the same. The largest difference is in the energy and it is about 20 %.

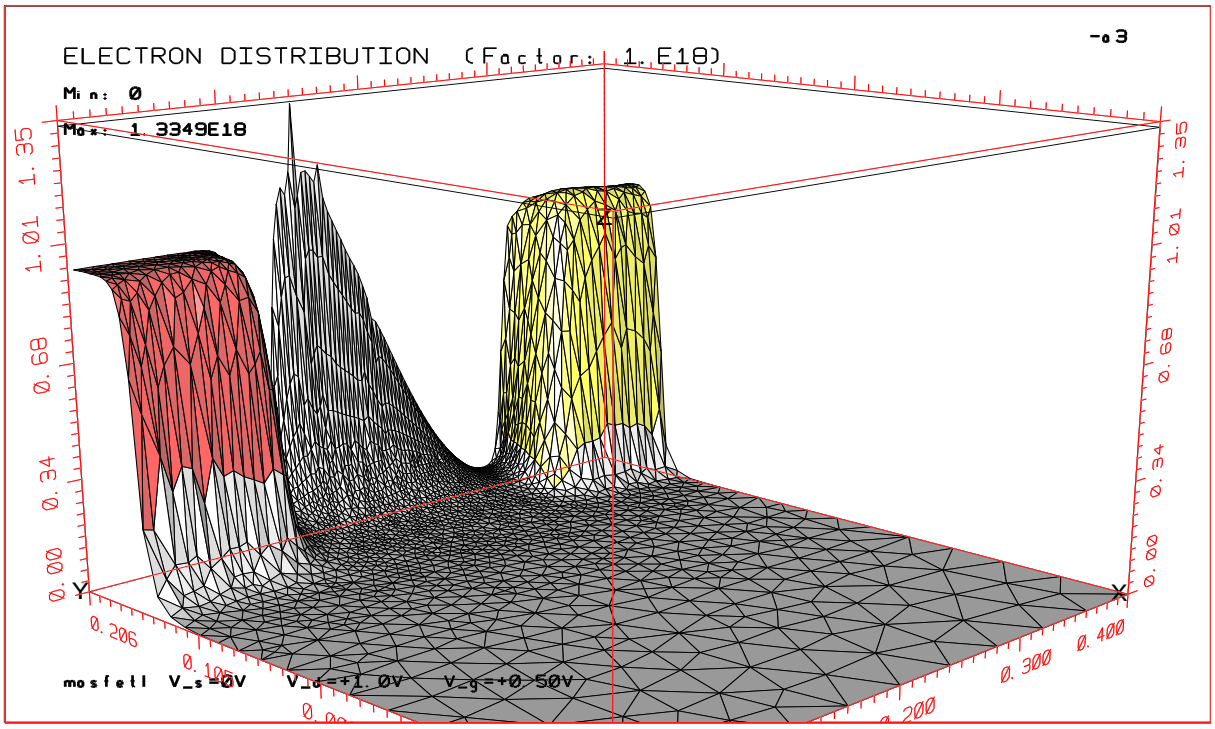

Figure 12: Stationary solution for the electron density in MOSFET (cm^{-3}).

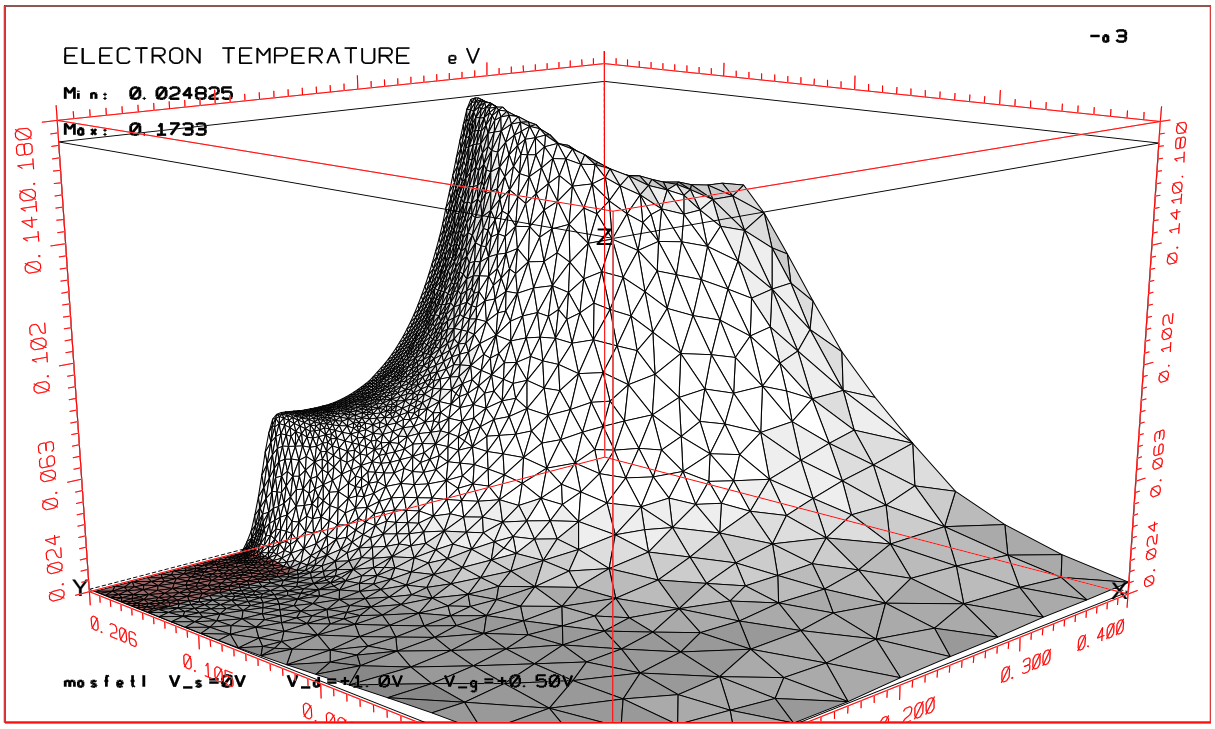

Figure 13: Stationary solution for the electron temperature in MOSFET (eV).

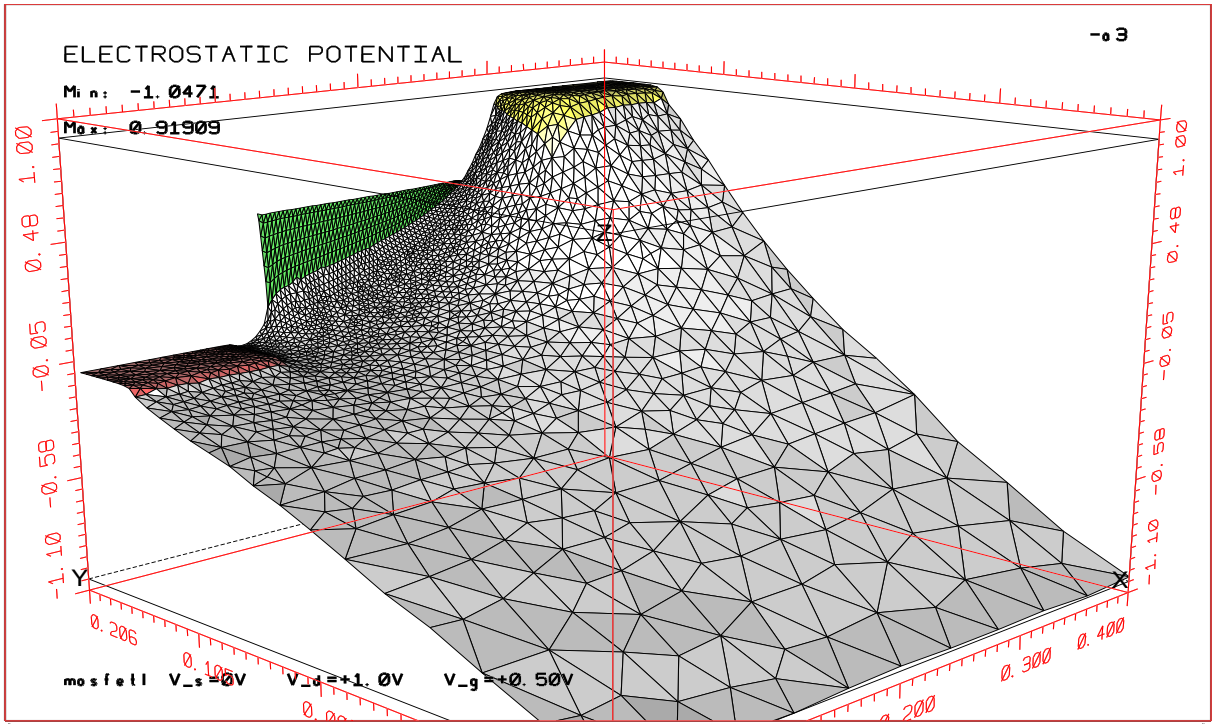

Figure 14: Stationary solution for the electrostatic potential in MOSFET (Volt).

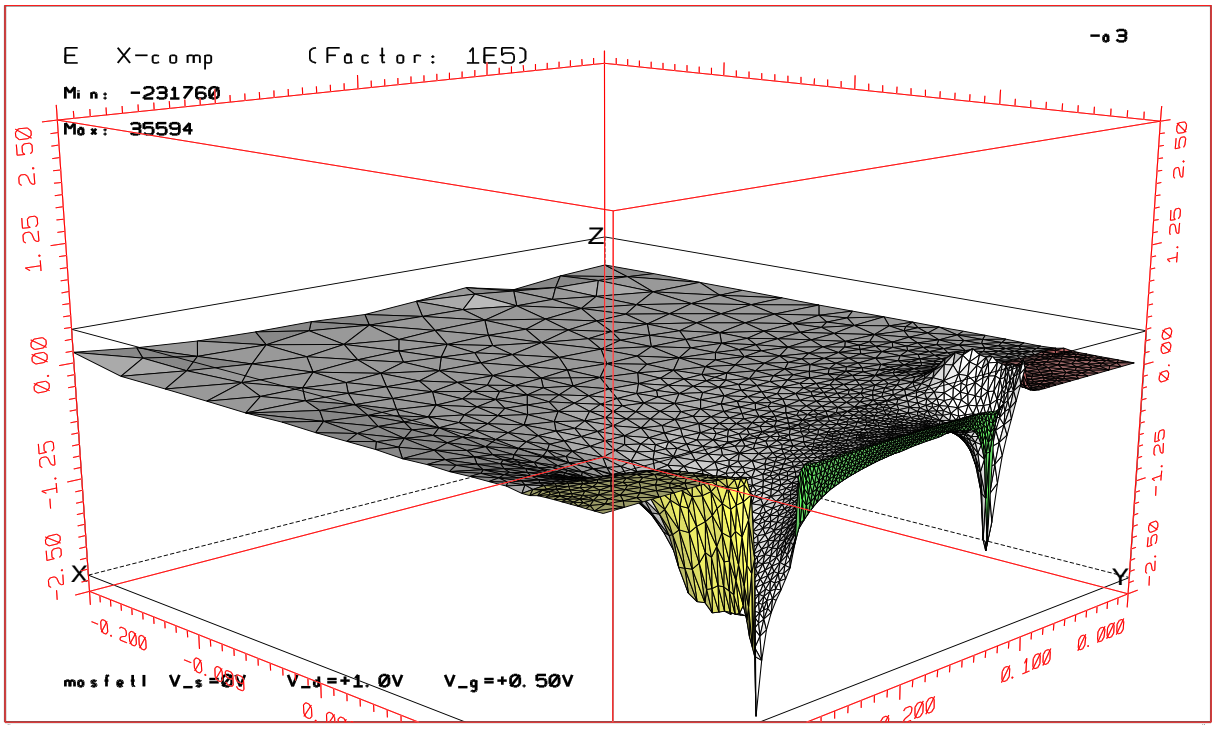

Figure 15: Stationary solution for the x-component of the electric field in MOSFET (Volt/cm).

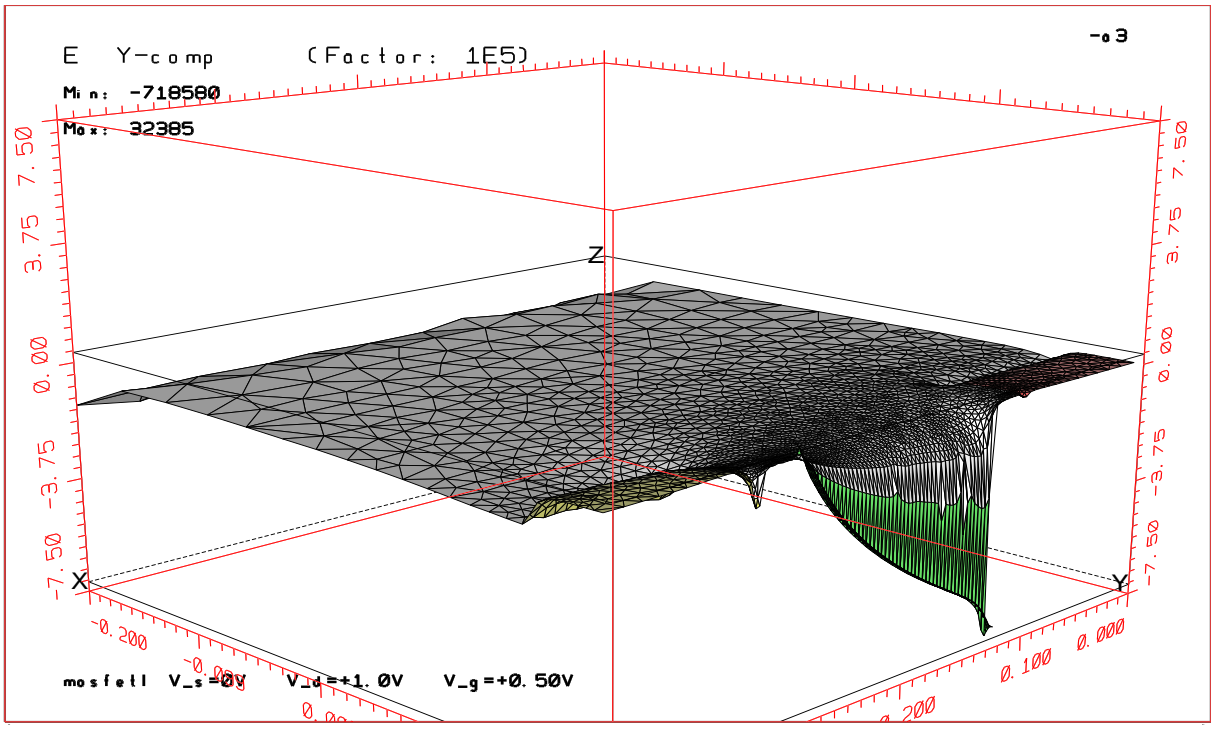

Figure 16: Stationary solution for the y-component of the electric field in MOSFET (Volt/cm).

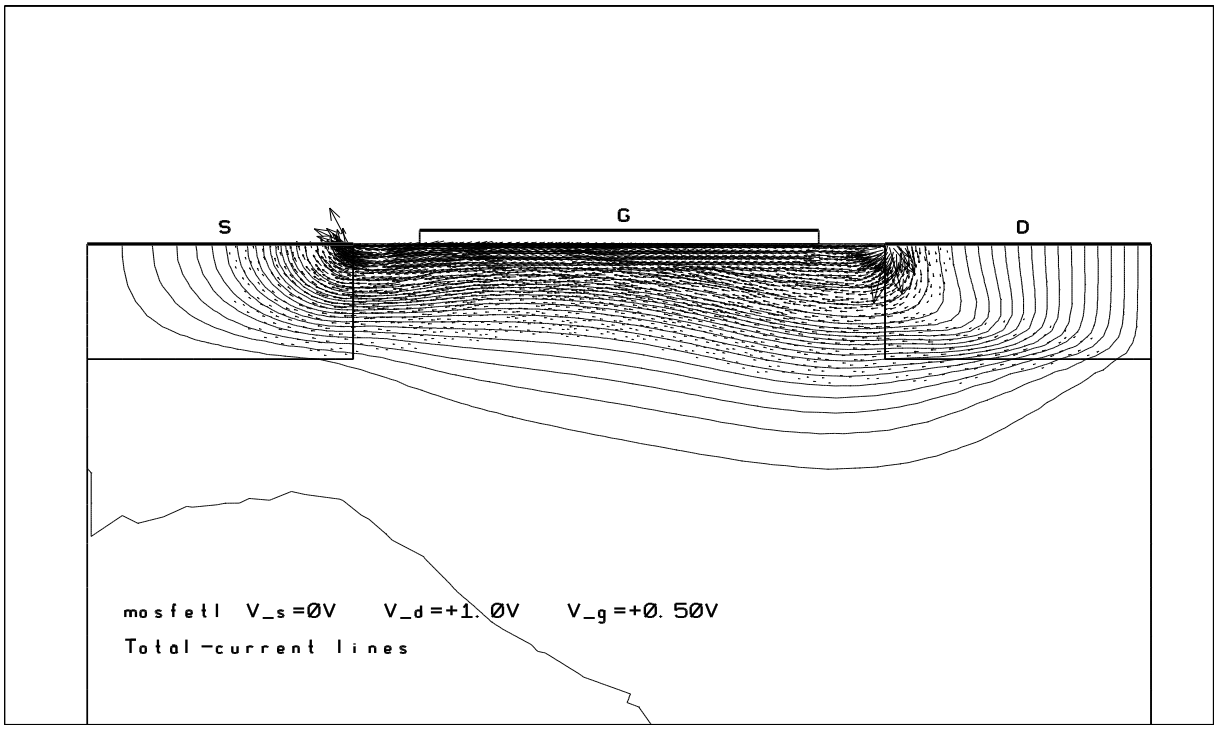

Figure 17: Current lines in MOSFET for the MEP model.

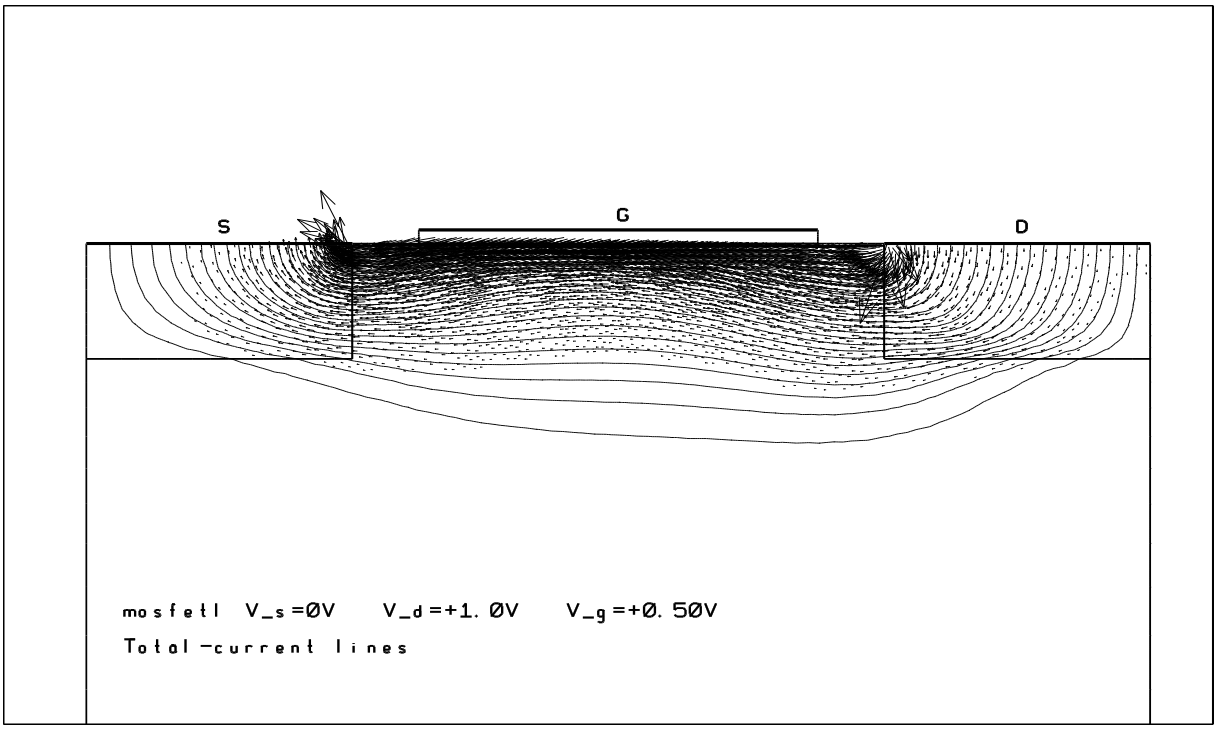

Figure 18: Current lines in MOSFET for the Stratton model.

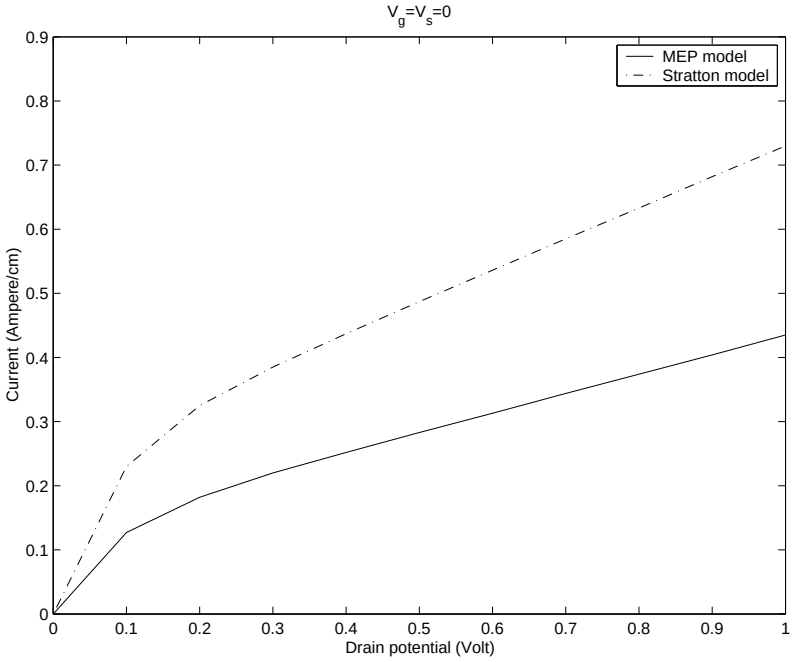

Figure 19: Characteristic curve for the MOSFET. $I_S(V_{DS})$ at $V_G = 0$.

Computed Source current I_s For the MOSFET							
Applied voltage			meshes and currents (A/cm)				
V_d	V_s	V_g	mesh 1 1198 el.	mesh 2 2521 el.	mesh 3 4644 el.	mesh 4 6094 el.	mesh 5 9796 el.
0.1	0.	0.	0.12245	0.12526	0.12722	0.12748	0.12740
0.2	0.	0.	0.17631	0.18050	0.18278	0.18307	0.18273
0.3	0.	0.	0.21275	0.21792	0.22038	0.22067	0.22015
0.4	0.	0.	0.24416	0.25017	0.25282	0.25311	0.25244
0.5	0.	0.	0.27392	0.28074	0.28358	0.28387	0.28307
0.6	0.	0.	0.30315	0.31079	0.31382	0.31410	0.31317
0.7	0.	0.	0.33224	0.34071	0.34393	0.34420	0.34314
0.8	0.	0.	0.36139	0.37068	0.37412	0.37439	0.37320
0.9	0.	0.	0.39071	0.40083	0.40450	0.40476	0.40345
1.0	0.	0.	0.42022	0.43120	0.43509	0.43534	0.43393
1.0	0.	0.25	1.0192	1.0406	1.0522	1.0535	1.0540
1.0	0.	0.50	1.7228	1.7555	1.7772	1.7798	1.7835

Table 3: Comparison of the computed source current for several meshes. The total computing time was less than 6' 30" for mesh 1 and about 18' for mesh 2 on the laptop computer.The various figures presented are relative to mesh 3.

Conclusions and Acknowledgments

The MEP energy-transport model for charge transport in semiconductor is free of any fitting parameters and it is based on sound and consistent physical principles. In the present article it has been shown, at least in the parabolic band case, that it can be used for CAD purposes simulating a 2D MESFET and a 2D MOSFET. The numerical integration is based on a mixed finite element method which is very robust, guarantees accurate current conservation and is able to deal with complex geometry.

The extension of the method to deal with the case of energy band described by Kane's dispersion relation is under current investigation by the authors.

The authors A.M.A.,V.R. and J.M.S. acknowledge the financial support by M.I.U.R (COFIN 2002 *Problemi Matematici delle teorie cinetiche*), P.R.A. (ex 60 %) and CNR (Agenda 2000 grant CNRG000DB75 and grant n. 00.00128.ST74).

References

[1] P. A. Raviart and J. M. Thomas, A mixed finite element method for 2nd order elliptic problems. In Mathematical Aspecys of Finite Element methods (I. Galligani and E. Magenes editors), Lecture Notes 606, Springer-Verlag 1977, pp. 292-375.

[2] A.M. Anile, V.Romano. Non parabolic band transport in semiconductors: closure of the moment equations, Continuum Mech. Thermodyn. (1999) 11:307-325, Springer-Verlag 1999.

[3] V.Romano. Non parabolic band transport in semiconductors: closure of the production terms in the moment equations, Continuum Mech. Thermodyn. (2000) 12:31-51, Springer-Verlag 2000.

[4] V.Romano. Non-parabolic band hydrodynamical model for silicon semiconductors and simulation of electron devices, Math. Meth. Appl. Sci. (2001), 24:439-471, John Wiley and Sons, Ltd. 2001.

[5] V.Romano. 2D simulation of a silicon MESFET with a nonparabolic hydrodynamical model based on the maximum entropy principle, J. Comp. Phys. (2002) 176: 70-92.

[6] A.Schenk. *Advanced Physical Models for Silicon Device Simulation.* Springer Wien New York.

[7] Ph. Montarnal. Modèles de transport d'énergie des semi-conducteurs, études asymptotiques et résolution par éléments finis mixtes. Thèse de doctorat, Université Paris VI, oct. 1997.

[8] A. Marrocco, Ph. Montarnal. Simulation des modèles energy-transport à l'aide des éléments finis mixtes. C.R. Acad. Sci. Paris, Vol.323, Serie I, 535-541, 1996.

[9] Ben Abdallah, N., Degond, P., and Genieys, S., 'An energy-transport model for semiconductors derived from the Boltzmann equation', *J. Stat. Phys.* **84** (1996) 205-231.

[10] Ben Abdallah, N., and Degond, P., 'On a hierarchy of macroscopic models for semiconductors', *J. Math. Phys.* **37** (1996) 3306–3333.

[11] D. Chen, E. C. Kan, U. Ravaioli, C-W. Shu, R. Dutton, *An improved energy-transport model including nonparabolicity and non-maxwellian distribution effects*, IEEE on Electron Device Letters, 13:26–28 (1992).

[12] E. Lyumkis, B. Polsky, A. Shir and P. Visocky, *Transient semiconductor device simulation including energy balance equation*, Compel 11: 311–325 (1992).

[13] R. Stratton, *Diffusion of hot and cold electrons in semiconductor barriers*, Phys. Rev., 126 (1962), pp. 2002–2014.

[14] Ashcroft N W and Mermin N D (1976), Solid State Physics, Philadelphia, Sounders College Publishing International Edition

[15] S. R. de Groot and P. Mazur, *Non Equilibrium Thermodynamics*, (Dover Publications Inc.,), New York, (1985)

[16] G. Mascali and V. Romano, Si and GaAs mobility derived from the hydrodynamic model of semiconductors based on the maximum entropy principle, preprint 2003.

[17] F. Brezzi, M. Fortin. Mixed and Hybrid Finite Element Methods. Springer Series in Computational Mathematics 15, Springer-Verlag (1991).

[18] R. Glowinski, P. Le Tallec. Augmented Lagrangian and Operator Splitting Methods in Nonlinear Mechanics, SIAM, Studies in Applied Mathematics, Philadelphia, 1989.

[19] Ch. Faure, Y. Papegay. Odyssée user's guide, version 1.7. Rap. Tech., R.T.0224., Sept.1998.

[20] J. W. Jerome and C-W. Shu, *Energy models for one-carrier transport in semiconductor devices*, in *Semiconductors part II*, The IMA volumes in Mathematics and its Applications, N. M. Coughran, J. Cole, P. Lloyd, J. K. White editors (1994), pp. 185–207.

[21] S. Selberherr, *Analysis and simulation of semiconductor devices*, Wien - New York, Springer-Verlag, 1984.

Unité de recherche INRIA Rocquencourt
Domaine de Voluceau - Rocquencourt - BP 105 - 78153 Le Chesnay Cedex (France)

Unité de recherche INRIA Lorraine : LORIA, Technopôle de Nancy-Brabois - Campus scientifique
615, rue du Jardin Botanique - BP 101 - 54602 Villers-lès-Nancy Cedex (France)
Unité de recherche INRIA Rennes : IRISA, Campus universitaire de Beaulieu - 35042 Rennes Cedex (France)
Unité de recherche INRIA Rhône-Alpes : 655, avenue de l'Europe - 38330 Montbonnot-St-Martin (France)
Unité de recherche INRIA Sophia Antipolis : 2004, route des Lucioles - BP 93 - 06902 Sophia Antipolis Cedex (France)

Éditeur
INRIA - Domaine de Voluceau - Rocquencourt, BP 105 - 78153 Le Chesnay Cedex (France)
http://www.inria.fr
ISSN 0249-6399